A Neuromechanical Model for Examining Viscoelastic Properties and Scaling Effects on Locomotion in a Rat Hindlimb

Fletcher Young

Abstract

This work first presents a neuromechanical model of a rat hindlimb with a complete musculature that has been validated against two existing rodent models. Next, I discuss the development of baseline parameters for the Animatlab muscle models. I then propose a manuscript that explores the impact of hindlimb scaling on neural control strategies employed during swing phase. Finally, I propose a manuscript dedicated to understanding how viscoelastic parameters in the hindlimb reject types of perturbations, and the specializations that segments of the leg have taken to aid in reducing the impact of perturbations. To better understand how the nervous system utilizes coordinates a complex viscoelastic system, I will:

Aim 1 - Create and validate a kinematic model of a rat hindlimb with a complete musculature. A many-muscled model will be developed that includes all major muscles in the rat hindlimb. The mechanical advantage of muscles will be validated against existing rodent models by comparing muscle moment arm profiles over joint range of motion. An analysis on the influence of biarticular muscles during nominal walking will be performed to determine what influence biarticular muscles have on the joints they span. Finally, a sensitivity analysis will be performed to determine the influence that muscle attachments points have on moment arm profiles.

Aim 2 – Characterize the viscoelastic parameters for the hindlimb by exploring how passive forces develop over stride at different limb scales. Baseline viscoelastic muscle parameters will be developed from experimental data on passive limb motion. I will develop a routine for calculating muscle forces in order to recreate a desired hindlimb motion. Finally, I will scale the limb and compare passive force profiles during swing phase.

Aim 3 – Investigate how viscoelastic properties allow the rat hindlimb to respond to perturbations of variable size and speed. This work will examine how the viscoelastic properties of individual muscles and muscle groups are suited to responding to perturbations. Perturbations will be characterized based on their speed and magnitude. By examining the transient response of the hindlimb, I will determine which areas of the limb are specifically suited for different kinds of perturbations.

Project Motivation

An animal's nervous and muscular system coordinate activity within an ever-present external environment. The inertial and viscoelastic properties of the body act as a kind of transfer function from neural activation to environmental manipulation (Full and Koditschek 1999). The environment, in turn, can dramatically alter this physiological transfer function as it carries out adaptive behavior (Chiel, Beer, and Sterling 1988; Pfeifer, Lungarella, and Iida 2007). By analyzing the interconnected nature of form and function, it may be possible to better understand how nervous systems allow animals of different sizes to engage in tasks across a range of body sizes and task speeds.

Contemporary biomechanical models often simulate *either* the nervous system or the musculature. These models fail to capture the complex interconnections between the different subsystems that are fundamental to understanding the complete pathway from neural activation to environmental manipulation (Chiel and Beer 1997; Chiel et al. 2009). These models, which serve as the basis for both biological research and robotic design, are most valuable when they provide a holistic interpretation of the animal and the environment it inhabits.

A simulation tool called Animatlab (Cofer, Cymbalyuk, Reid, et al. 2010) has been used to create neuromechanical models of animals such as a praying mantis (Szczecinski et al. 2017), a rat (Hunt et al. 2015), and a locust (Cofer, Cymbalyuk, Heitler, et al. 2010). Animatlab is uniquely suited to study the interplay of different body systems because it allows a user to model both a biomechanical physics environment as well as a neural control system. This makes it possible to actuate a model in a 3D physics environment by coordinating neural activations, as well as map reflexive pathways back from the environment into the nervous system.

A focus of current work is to use Animatlab to test how the nervous system controls groups of muscles to carry out tasks. Specifically, we would like to know how the relationship between the size of an animal and the speed of the tasks it carries out relate to one another. What accommodations does a nervous system have to make to move a large, heavy limb quickly? How do perturbations influence the passive motion of a limb? What kinds of perturbations can limbs reject? A complex neuromechanical model would help us develop insight to these questions.

Aim 1 - Create and validate a kinematic model of a rat hindlimb with a complete musculature.

This work builds off of a neuromechanical model developed by Dr. Alexander Hunt in completion of a doctoral thesis (Hunt et al. 2014; 2015; Hunt 2016). Hunt's rat model, shown in Figure 1, included a simulated nervous system that coordinated hindlimb muscles to emulate locomotion in a nominal environment using discrete subunits known as central pattern generators (CPGs) (Beer, Chiel, and Gallagher 1999; McCrea and Rybak 2008). This work presented a novel method for tuning neural parameters for feedback systems to induce self-supported walking.

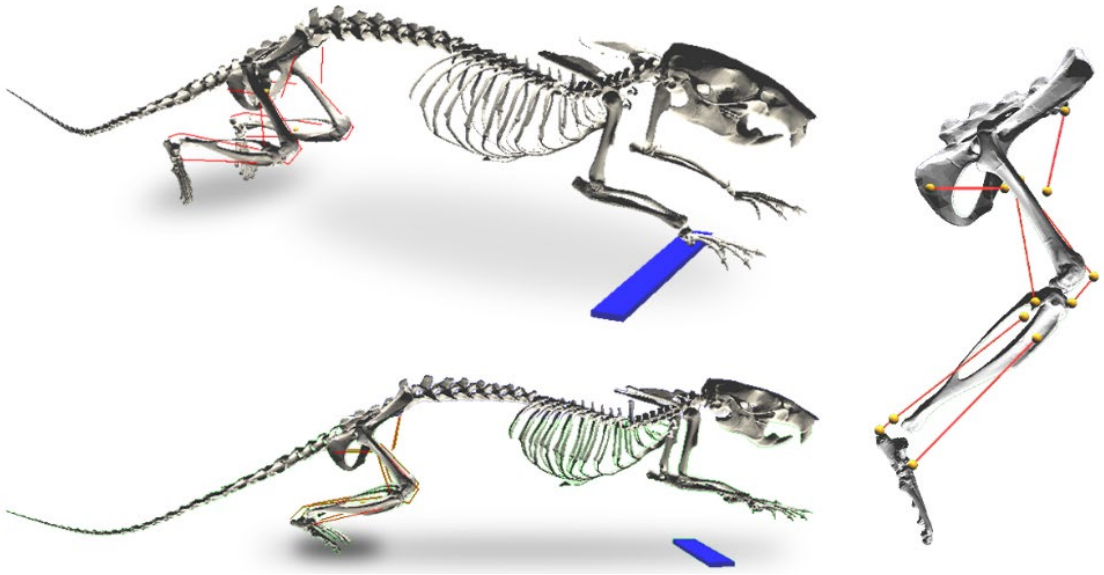

Figure 1 Hunt's rat model. The torso and upper limbs are held stationary above the ground as the hindlimb muscles coordinate locomotion. Red lines indicate muscle paths and yellow markers represent muscle attachment points.

In order to explore how a more generalized nervous system configuration, it is necessary to create a hindlimb model with a complete musculature. Hunt's model used a reduced muscle set with a flexor-extensor pair at each joint. Muscle pairs were directly mapped to the two halves of a CPG whose oscillation patterns were hand-tuned to recreate walking-like motion by moving the joint.

Hunt's model makes many simplifications to the rat physiology that hinder our ability to explore interplay between physiology and the environment. In particular, this model fails to capture the complex nature of biarticular muscles (i.e. muscles that span two joints), whose torque profiles are not isolated to individual joints. The first step to enhancing Hunt's model is to incorporate biarticular muscles and then validate their mechanical advantage against other existing models. **The goal of this aim is to create a biomechanical model of the rat hindlimb that includes all major muscles, physiologically representative muscle paths, and is validated against existing rodent hindlimb models.**

<u>Sub Aim 1.1: Develop physiological lines of action for all hindlimb muscles</u>

Muscle lines of action in the model are based on anatomical drawings and descriptions from E.C. Greene's 1955 publication Anatomy of the Rat (Greene 1955). Greene's work is a primer on rat anatomy that includes hundreds of detailed anatomical drawings and descriptions of rat musculature, nervous system, and circulatory system. Of particular interest to this work are the detailed descriptions of muscle attachment points to bone structures, their relationships to neighboring muscles, and the paths of tendons around joints.

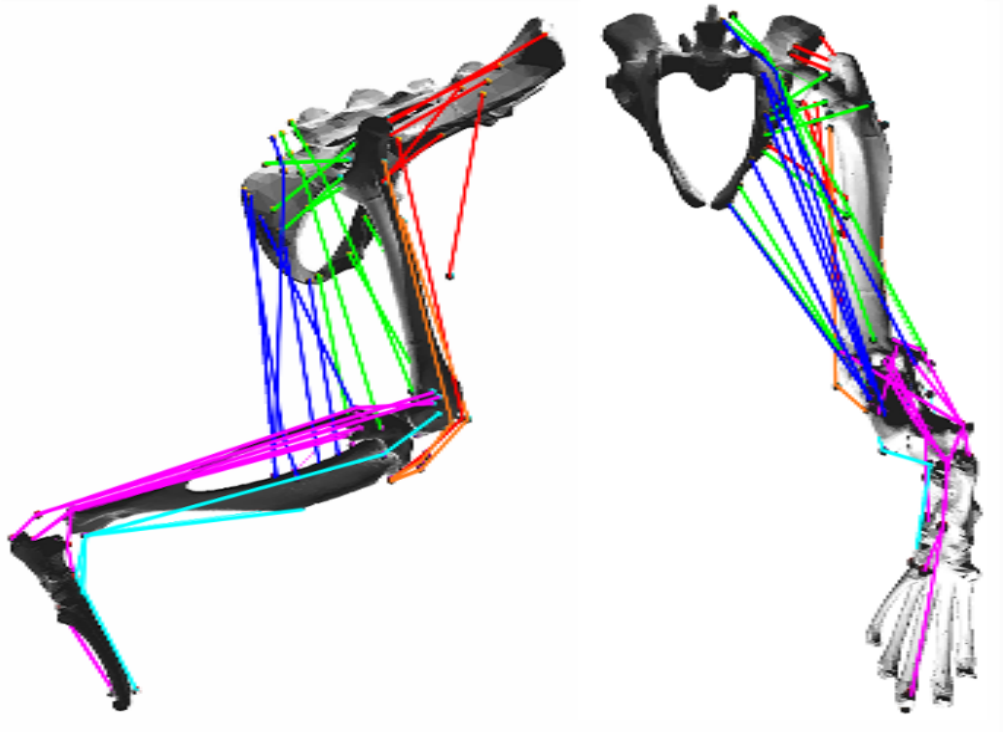

Figure 2 A neuromechanical model of the rat hindlimb developed in Animatlab with thirty-eight muscles. Colored lines represent muscle lines of action, muscle attachments are shown as small spheres. Colors denote general muscle grouping for visual clarity but do not have a functional significance. Muscle attachment points not directly on a bone surface represent soft tissue attachment.

In simulation, lines of action are created by affixing muscle attachment points onto a 3D rat skeleton. Attachment points (small spheres in Figure 2) remain static in bone-centric reference frame and represent either muscle-bone connections or "via points" to approximate curved muscle paths. Via points were added to muscles such that their lines of action never pass through bone throughout the limb's range of motion. For muscles that attach to bones along a line of attachment (e.g. the gluteus maximus attaching to the dorsal border of the ilium), a single attachment point was placed approximately halfway along the line of attachment.

Simple hinges were used for the joints with limits set to allow for motion within physiologically plausible regions. Joint centers are stationary relative to the proximal bone and were set such that the distal bone does not collide with other bones throughout the limb's range of motion.

Publication

1. Young, F., Hunt, A. J. & Quinn, R. D. A Neuromechanical Rat Model with a Complete Set of Hind Limb Muscles. in Biomimetic and Biohybrid Systems 527–537 (Springer, 2018).

Sub Aim 1.2: Compare model kinematics to existing rodent models from the literature

With muscle lines of action applied to the model, it was important to validate the model against some existing rodent models (Charles et al. 2016; Johnson et al. 2011). One method for comparing models is to examine muscle moment arm profiles throughout joint ranges of motion. Of particular interest are the differing mechanical advantages of biarticular muscles across each of their spanned joints during nominal locomotion.

Moment arms are a representation of the mechanical advantage a muscle has about a joint (Visser et al. 1990; Lee et al. 2008; Williams et al. 2008; Yeo et al. 2011; Charles et al. 2016). Understanding the mechanical advantage of muscles is important for understanding the force contributions a muscle can make throughout motion. Moment arm profiles (the length of a muscle's moment arm about a joint over its range of motion) are a useful metric whereby a model can be validated against existing hindlimb models.

A routine was developed in Matlab (Mathworks, Natick, MA) for calculating moment arm lengths for all muscles when the leg is set to an arbitrary limb configuration. Moment arms were developed using vector analysis, shown in Figure 3, where the muscle is projected onto an orthogonal plane to the joint axis. The moment arm is defined as the perpendicular distance from the joint to a single muscle segment, called the free muscle segment. The free muscle segment represents the part of the muscle that undergoes active length change throughout joint motion. By "driving" the limb with motors placed at the joints, it is possible to develop muscle moment arm profiles over a full joint range of motion.

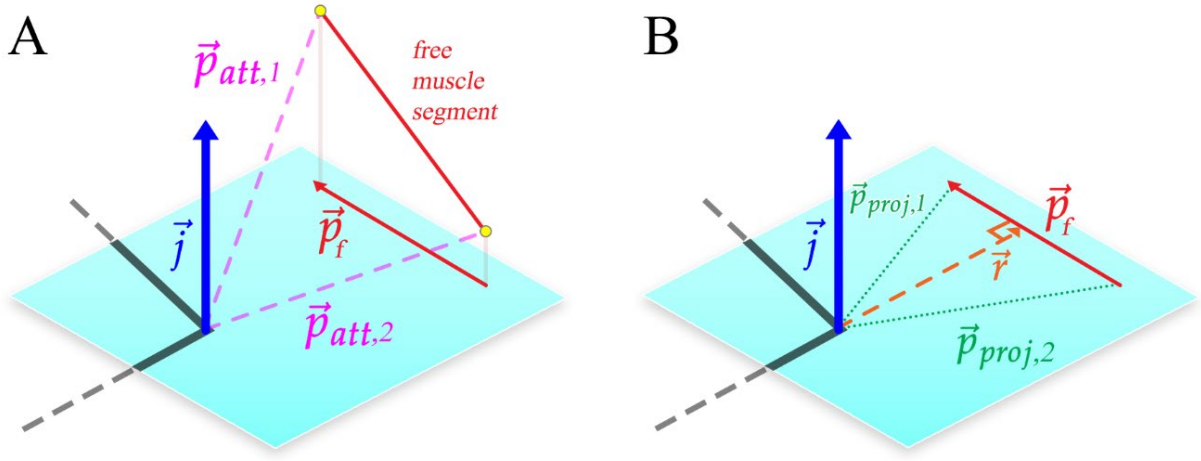

Figure 3 The calculation process for muscle moment arms using vector analysis. **A)** The endpoints of the free muscle segment, $\vec{p}_{att,1}$ and $\vec{p}_{att,2}$,are projected onto the plane orthogonal to the joint axis, $\vec{j}$. **B)** The moment arm, $\vec{r}$, is the length of the perpendicular segment from the joint to the projection of the free muscle segment, $\vec{p}_f$.

A subset of moment arm profiles has shown a comparable magnitude, range, and shape to the Johnson rat model and the Charles mouse model. Moment arm profiles are normalized with respect to the length of the tibia in order to compare the two rodents. In general, the model showed strong agreement to the results from Charles but differed notably from the Johnson model for the pectineus, semimembranosus, and vastus intermedius (Figure 4 B-D). The exact reasons for this are difficult to determine because the process for Johnson's moment arm calculation is not well defined.

One reason for considering the validity of the Charles moment arms over the Johnson moment arms is that the process for developing muscle paths in the Animatlab is more similar to Charles' approach. Charles implements via points to guide muscles about bone structures whereas Johnson apparently does not use wrapping objects or via points when developing their muscle paths. Constraints on the muscle path are likely to have a large impact on the moment arm profiles (O'Neill et al. 2013).

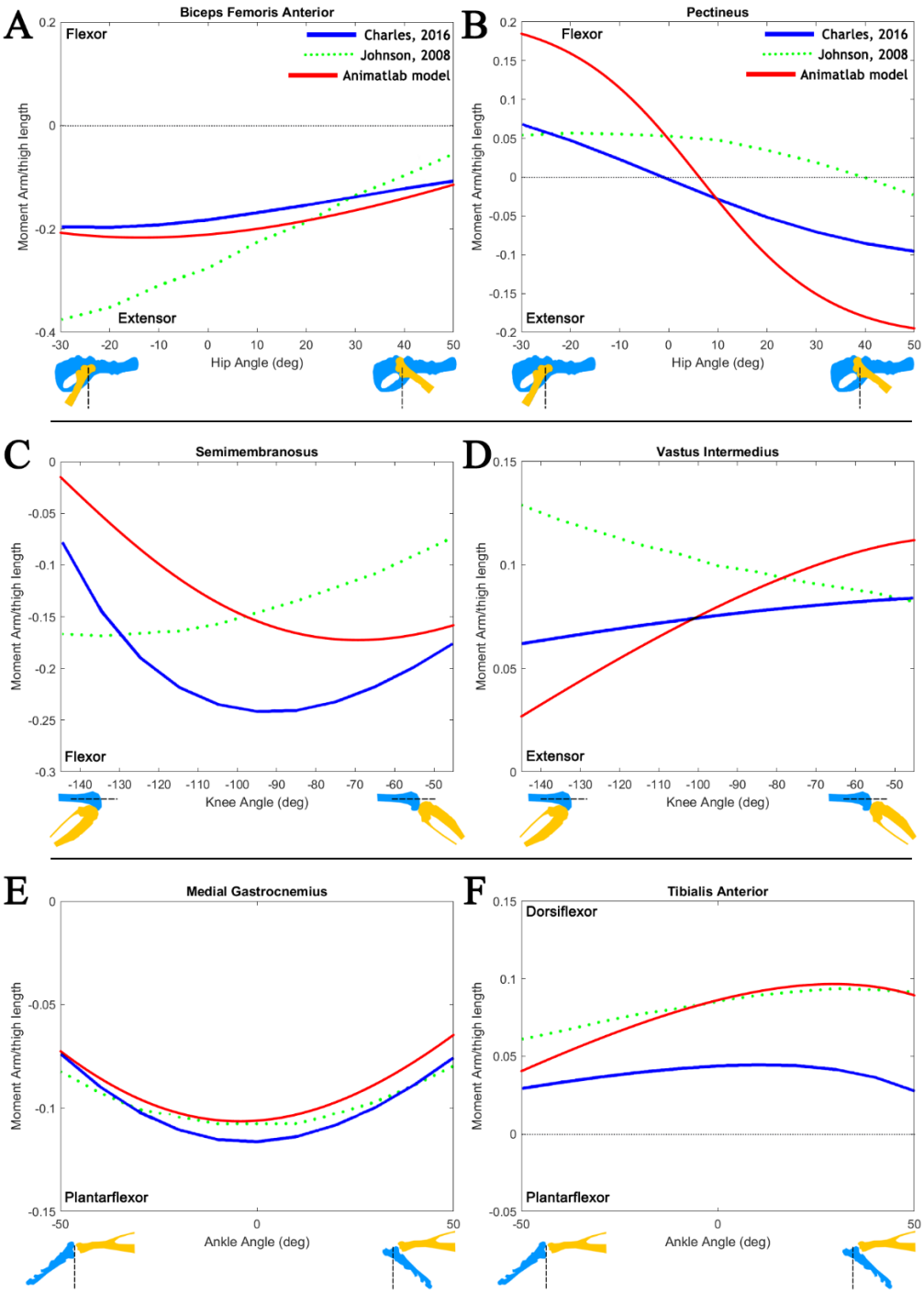

Figure 4 Moment arm profiles for select muscles in comparison to two existing rodent models. **A)** The biceps femoris anterior is a hip extensor whose mechanical advantage about the hip is nearly constant **B)** the pectineus changes from a hip extensor to a flexor due to its origin lying almost directly below the hip itself. It should be expected that when the hip is at about 0°, the pectineus would change its function **C)** the semimembranosus is a biarticular muscle that acts as a knee flexor **D)** the vastus intermedius is part of the group of muscle which insert into the tibial tuberosity and extend the knee **E)** the medial gastrocnemius is an ankle plantarflexor **F)** the tibialis anterior is an ankle dorsiflexor.

Sub Aim 1.3 Demonstrate the difference between moment arm profiles for biarticular muscles about their spanned joints

Biarticular muscles are important because they play a complex role in regulating non-sagittal forces, distribute energy between joints, and improve efficiency in motions where the force and movement are in different directions (Hof 2001). An example of how the mechanical advantage of biarticular muscles differs between its spanned joints is shown in Figure 5 as a 3D surface. Between touch down and lift off during nominal locomotion, the biceps femoris posterior (BFP) must contend with two very different mechanical advantages. However, about the knee, the BFP is able to maintain the same mechanical advantage despite changing its value throughout swing.

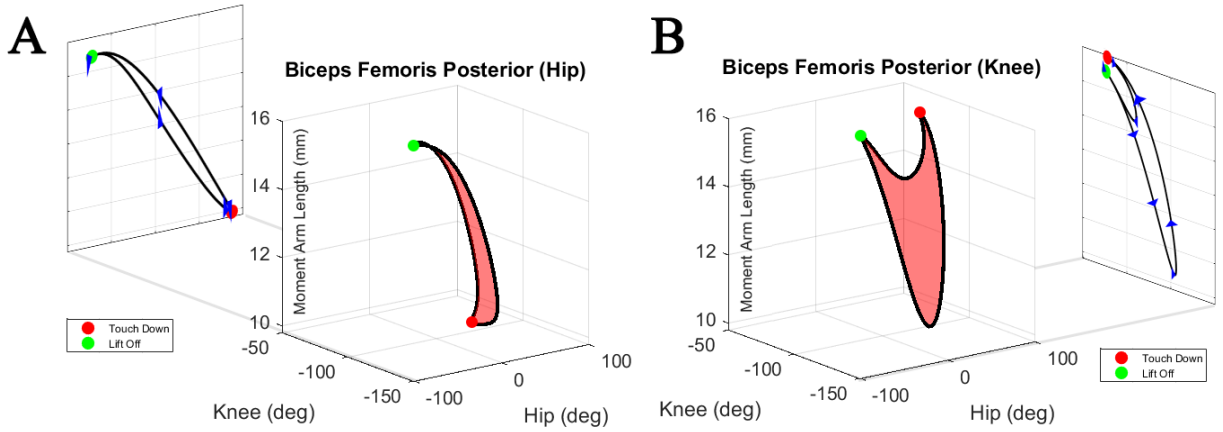

Figure 5 Moment arm profiles for the BFP across the hip and the knee. **A)** Across the hip, the BFP has different has a small mechanical advantage at touch down but a large advantage at lift off. **B)** For the knee, the BFP has a similar mechanical advantage at touch down and lift off.

The variable nature of biarticular muscle advantage suggests that, for sagittal plane walking, muscle contributions change independently for spanned joints. Incorporating biarticular muscles into existing bi-modal CPG systems like Hunt's model requires a method be developed for integrating these joint-specific responses of biarticular muscles.

In addition to calculating moment arm profiles, a sensitivity analysis was conducted to examine the impact of muscle attachment point placement on sagittal plane moment arm profiles. The sensitivity analysis showed that moment arm profiles were robust in shape and magnitude when changing the attachment points bounding the free muscle segment.

Publications

1. Young, F., Rode, C., Hunt, A. & Quinn, R. Analyzing Moment Arm Profiles in a Full-Muscle Rat Hindlimb Model. Biomimetics 4, 10 (2019).

Aim 2 – Characterize the viscoelastic parameters for the hindlimb by exploring how passive forces develop over stride at different limb scales.

Recent work shows that animals at different sizes utilize control strategies that are unique to their length scale (Vogel 2005; Hooper 2012; von Twickel et al. 2019). For example, by measuring muscle activation levels in a stick bug, we can see that the animal engages muscles throughout the entirety of swing to bring the leg forward (Hooper et al. 2009). In contrast, measurements in horses show that there is very little neural control in early swing phase, presumably because the horse uses inertia to "throw" its leg forward (Hooper 2012). These two different control strategies illustrate the broader concept that animal nervous systems have adapted to navigating the world differently depending on the size of the animal. **The goal of this aim is to develop passive properties for all muscles in the hindlimb and compare how passive force distribution changes with respect to scale.**

Sub Aim 2.1: Develop length-activation parameters for all muscles

The development of muscle parameters falls into two categories: length-activation profile parameters and viscoelastic parameters. Two tension relationship curves dictate the force generating capabilities of the linear Hill (Hill Archibald Vivian 1938) model: the length-tension (LT) curve and the stimulus-tension (ST) curve. These curves are represented by the terms A_l and A_m in Equation 1. The LT-curve relates a muscle's force-generating capabilities at various isometric lengths while the ST-curve relates the membrane potential to force output.

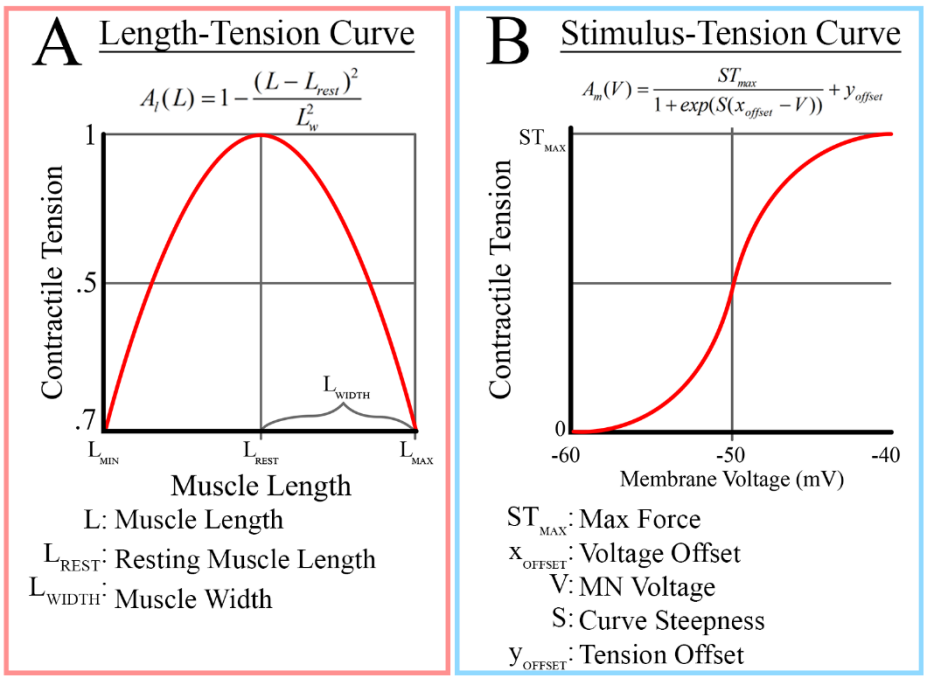

Figure 6 A) The length-tension curve defines the ability of muscle activation to generate tension at different muscle lengths. The output of this curve ranges from [0,1]. **B)** The stimulus-tension curve relates motoneuron activation to the tension in the muscle. The output range of this curve is [0, ST_{max}].

The LT-curve (Figure 6A) relates the maximal tension generating capability of muscle at different lengths, where the muscle is capable of generating the maximum possible force at its

resting potential. The resting length for muscles is determined by moving the leg through its full range of motion (i.e. from L_{min} to L_{max}) and finding the midpoint between these values. The muscle width is set such that at the length extremes the muscle is capable of generating 70% of its maximum tension (Zajac 1989).

The ST-curve (Figure 6B) relates the motoneuron activation to muscle tension. No tension is generated at a resting potential of -60mV, while at full activation (-40mV) the muscle generates a maximal contractile force, ST_{max}. ST_{max} is set such that at steady state, the activation term is capable of generating its maximum tension, F_{max}. Calculating the value of ST-curve parameters, ST_{max} and y_{off}, is described in the supplementary material.

Sub Aim 2.2: Calculate baseline viscoelastic parameters for all muscles

Animatlab uses a two-compartment muscle model (Figure 7) with an elastic spring element (K_{SE}) representing connective tissue in series with a damping element (B), parallel spring element (K_{PE}), and a contractile element (A) in parallel. Physiological parameters for rat hindlimb muscles exist in the literature (Johnson et al. 2011; Eng et al. 2008) but efforts to fit these values to the model could not converge to stable solutions. Values for the maximum tension, F_{max}, are taken from Johnson 2011.

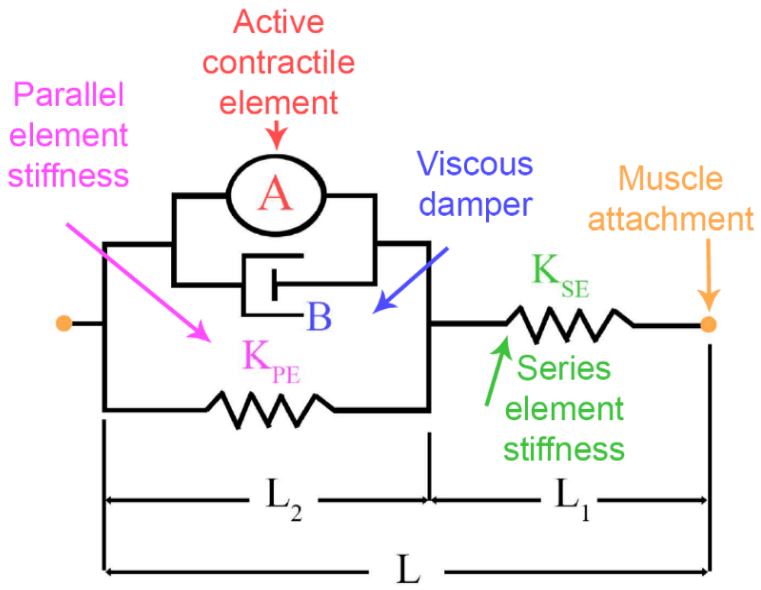

Figure 7 The linear Hill muscle model implemented in Animatlab. The force generating component, A, is composed of a length-tension and stimulus-tension term. Circular ends represent muscle attachment points connected to bone meshes.

The nonlinear tension of the Hill model has been formalized (Shadmehr and Arbib 1992) as,

$$\frac{dT}{dt} = \frac{K_{SE}}{B}\left(K_{PE}\left(L - L_{rest}\right) + B\frac{dL}{dt} - \left(1 + \frac{K_{PE}}{K_{SE}}\right)T + A_l A_m \right), \qquad (1)$$

where T is muscle tension, dt is the physics timestep, K_{SE} is series element stiffness, K_{PE} is parallel element stiffness, L is muscle length, B is the muscle damping, A_l is a dimensionless tension-length percentage, and A_m is muscle activation in Newtons.

The viscoelastic parameters (K_{SE}, K_{PE}, B) of all muscles in the limb are determined by fitting simulated joint motion to experimental hanging leg data. Collaborating with partners at Northwestern University, skin marker data has been recorded for freely hanging rat legs in which individual muscles are stimulated by electrodes. In Animatlab, I stimulate these same muscles and compare the resulting joint motion to experimental data. Through an optimization routine, I reduce the sum squared difference of the joint angle waveforms by changing the viscoelastic properties.

Sub Aim 2.3: Calculate muscle forces necessary to recreate motion

To recreate motion, it is necessary to develop force profiles for all muscles in the hindlimb. This is accomplished through a process in which the leg is driven through a desired leg trajectory and passive torques and moment arm profiles are measured. Passive torques include the passive tension generated by muscles and the gravitational weight of the limb segments. Moment arm profiles are generated as defined in Aim 1. Although not included in this work, it is possible to apply load torques that simulate the effects of ground reaction forces by treating the leg as a multi-segment arm with a force vector at the end effector (Murray, Li, and Sastry 1994).

Since force distribution is an infinite subspace (i.e. there are an infinite number of force values and combinations), different force optimization methods have been explored. Different force distribution cost functions have been explored and include minimizing the total muscle force (Pedotti, Krishnan, and Stark 1978; Penrod, Davy, and Singh 1974), stress (Crowninshield and Brand 1981), activation (Kaufman et al. 1991), and fatigue (Prilutsky and Zatsiorsky 2002). An optimization cost function was selected from Pedotti's work, $J = \sum_{i=1}^{38} \left(\frac{F_i}{F_{max}} \right)^2$, due to its ability to create smooth tension profiles that minimized spontaneous muscle switching.

At every timestep of the simulation, an optimization process is carried out to determine the muscle forces necessary to counteract the passive torques.

Sub Aim 2.4: Modify the Animatlab muscle model to correct for tension deadzones

While recording tension profiles in Animatlab, it became apparent that the tension calculations contain a small error that made predicting muscle forces difficult. There are regions of length and activation in Animatlab's default muscle tension model (Equation 1), where tension should be present but is not. This region, shown as the red surface in Figure 8, causes the tension profile to become discontinuous for valid length-activation values and misrepresents the passive response of muscle to length changes.

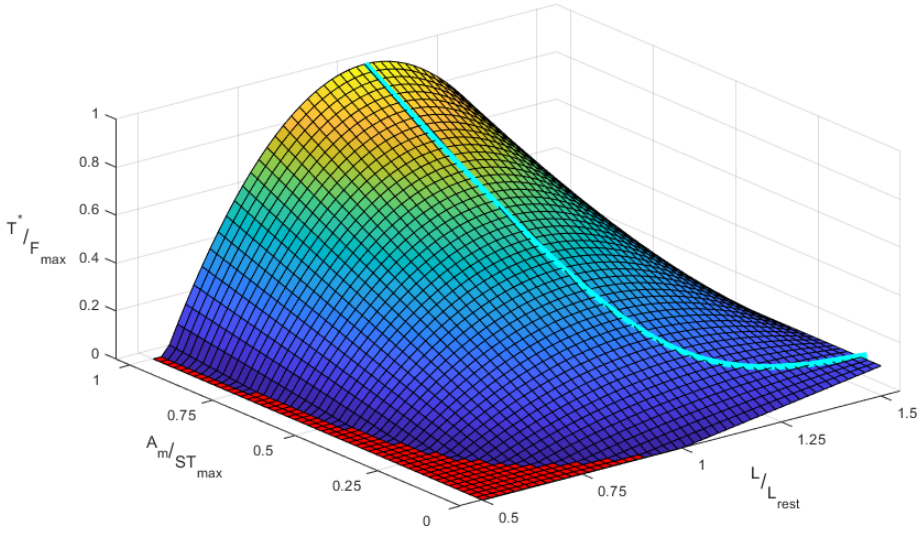

Figure 8. A surface representing the steady state tension of a muscle as a function of its length and activation. The red surface represents a tension deadzone, an area of length and activation that is incapable of generating tension despite both values being within valid ranges. The cyan line represents the maximum steady state tension with respect to length.

To determine the cause of tension deadzones, I examined the steady state muscle tension (T^*),

$$T^*(L, A_m) = \left(\frac{K_{SE}}{K_{SE} + K_{PE}} \right) \left(K_{PE} \left(L - L_{rest} \right) + A_l(L) A_m \right). \tag{2}$$

Tension deadzones are the result of allowing the passive length term, $K_{PE}(L - L_{rest})$, to generate negative values when the muscle is below its resting length. This is antithetical to the concept that muscles only generate contractile tension. At moderate values near the resting length, this error does not have a large effect. However, when the muscle is significantly below the resting length, it is possible that the "negativity" of the passive tension will counteract the "positivity" of the activation.

To correct tension deadzones, I modified the tension equation in Animatlab using the software developer kit. Specifically, I changed the muscle tension in Equation 1 to

$$\frac{dT}{dt} = \frac{K_{SE}}{B} \left(K_{PE} \lceil L - L_{rest}, 0 \rceil + B \frac{dL}{dt} - \left(1 + \frac{K_{PE}}{K_{SE}} \right) T + A_l A_m \right), \tag{3}$$

where $\lceil . \rceil$ denotes the ceiling function. This modification fixes the tension deadzone problem and prevents the muscle from generating negative passive tension. More detail on this correction is discussed in a 2020 Living Machines publication.

Publications

1. Young, F., Hunt, A., Chiel, H., & Quinn, R. Using Animatlab for Neuromechanical Analysis: Linear Hill Parameter Calculation. Living Machines 2020, (in print)

Sub Aim 2.5 Manuscript Proposal: Exploring the effects of viscoelastic properties on swing phase control in animals of different scales

Anecdotal observations indicate that at the end of swing phase in the rat, the vastus muscles (knee extensors) exhibit a burst of activity that is not seen in cats. Low level activation bursting in the rat seems to be present in the vastus lateralis in some work (Thota et al. 2005; Aoi et al. 2013; Sandercock et al. 2018) and is absent in cat EMGs (Prilutsky et al. 2015; Markin et al. 2012). This indicates that, perhaps, a rat nervous system must compensate for a lack of limb inertia by stimulating specific muscles. A possible broader implication for this observation is that the scale of an animal causes its nervous system to approach the same task in different ways to account for its body composition.

Swing phase of gait is a relatively simple limb task that has been shown to elicit different neural activation responses depending on the scale of an animal (Hooper et al. 2009; Hooper 2012; von Twickel et al. 2019). This makes it a useful activity for analyzing the impact that scaling properties have on nervous system demands. By analyzing the force demands from swing phase at different scales, we can make inferences into how the nervous system must behave in order to accommodate the proper motion. **The goal of this paper is to determine whether passive force profiles are predictably different during swing phase for animals of different scales**.

I hypothesize that a rat-sized model will show that propulsive muscles must be active for a relatively long duration of swing in order to pull the leg forward. In a cat-sized model, I would expect to see less propulsive muscle activity during swing phase compared to the rat. In a horse-sized model, I would expect to see braking forces during the latter part of swing in order to slow the limb down. This work would clearly demonstrate that the nervous systems of animals at different scales change their activity in a predictable manner in order to accommodate scale-dependent limb properties.

Aim 3 – Investigate how viscoelastic properties allow the rat hindlimb to respond to perturbations of variable size and speed.

Sub Aim 3.1 Manuscript Proposal: Study perturbation response in the hindlimb for passive response

The aggregate response of a limb is a combination of neural control, muscular properties, and environmental state (Nishikawa et al. 2007). This raises the question: What kinds of perturbations can a rat leg resist purely through its limb mechanics and what kinds would they need to compensate for with neural activation? **The goal of this paper is to examine how the viscoelastic properties of a rat hindlimb respond to perturbations at the size and speed that rats experience while walking.** I hypothesize that the baseline viscoelastic properties of the hindlimb are specifically suited to reduce reject perturbations at the size and speed that rats experience during walking.

Perturbation response is well studied as a method for understanding how environmental effects can be accommodated by using local reflex pathways (Torres-Oviedo, Macpherson, and Ting 2006). I expect that by changing the baseline viscoelastic makeup of the hindlimb, that it will cause the limb to experience long term effects from perturbations through the limb's inability to return to steady state (dynamic or static). For example, reducing the damping in hindlimb muscles may cause the limb to reject fast perturbations but not change the response to the size of the perturbation itself.

The use of the many-muscled model allows for high parametric fidelity in which viscoelastic parameters can be changed for individual muscle or for muscle groups. It would be possible to determine which areas of the hindlimb are primarily responsible for specific perturbation responses and to simulate the limb response if group parameters are changed or removed altogether.

This knowledge would be important to understanding control systems because VE parameters for different limb areas may be sensitive to a specific type of perturbation response. Some muscles may be sensitive to perturbation magnitude, which would highlight compensatory mechanisms in the nervous system that are necessary to resume normal motion. Other muscles may be sensitive to perturbation speed, which would highlight whether response come from faster lower level control systems or slower high level control systems.

The first step to studying this aim is to create an Animatlab physics testbed which would allow me to study the effect of different types of perturbations to the system. For external perturbations, this would involve creating a platform under the hindlimb toe that can be raised or lowered at desired amplitudes and frequencies. This would simulate impact collisions to the limb and allow me to study both the effects of changing the size and the speed of the perturbation. This work would compare limb response with respect to VE parameters in the limb. It would also be possible to make suggestions for VE parameter changes that would allow for a better response to the system, indicating areas where simplifications in the model may need to be reassessed.

Sub Aim 3.2 Possible Additional Exploration: Internal perturbations to the nervous system

An additional branch of consideration for this aim would involve applying neural perturbations to the system. This would involve moving the leg through a desired motion and injecting current at specific times and magnitudes to determine the effect on the hindlimb. This would require a system for creating a simple nervous system in Animatlab and developing routines for injecting currents in a meaningful way to elicit motor responses.

As we begin stimulating muscles through motoneurons in Animatlab's neural design simulator, it is helpful to develop tools that can rapidly modify large groups of neurons. I have developed a Matlab toolbox, called Canvas, that includes a library of Animatlab objects and their associated parameters. Object-oriented programming allows a user to add and connect neurons, create new synapse types, and generate charts to plot simulation results all within Matlab. Users are then able to generate either an Animatlab project (contains the interactive user interface) or a simulation file (for direct simulation results without visualizing the physics simulation).

Large networks, such as the multi-layer CPG networks for controlling limb locomotion, can include hundreds of Animatlab objects and thousands of individual connections. Canvas reduces the time required to hand-connect networks by allowing the user to implement these systems through routines as simple as a for-loop. The modular nature of Canvas also allows users to build their own pre-fabricated networks, allowing for rapid-deployment of complex subnetworks.

For this application, it would only be necessary to generate muscle motoneurons, perturbation stimuli, and output charts to measure muscle- or joint-level responses. Incorporating Canvas into this work to generate complex nervous systems could be an interesting tool but how it can be incorporated to its fullest extent is yet to be determined.

Supplementary Material

1. VE Parameter Optimization

To develop baseline VE parameters for the hindlimb muscles, we match experimental joint motion with simulated joint motion. This is accomplished by optimizing the parameters K_{se}, K_{pe}, and B for thirty-eight muscles to reduce the sum-squared difference between the simulated and experimental joint motion profiles.

In addition to matching experimental results, it is important that the VE parameters are selected such that they maintain the functional goals for muscles in Animatlab. For a maximal (20 nA) stimulus, we want the muscle to be capable of generating its maximum tension (F_{max}) while at steady state. When not stimulated (0 nA), the muscle tension should be purely passive ($A_m = 0$).

The optimizer for this process is the patternsearch function in Matlab. This process perturbs input values in a "mesh" pattern in order to find parameter combinations that reduce a cost function. Patternsearch is useful for problems that do not have a defined gradient, such as a simulation with discrete outputs. In addition to using the mesh polling method, a mesh adaptive direct search is included to increase effectiveness by performing an additional search step before polling for new values.

Linear constraints are applied to the optimizer to ensure that the tension profiles in Animatlab do not become asymptotically unstable. The discrete representation of the muscle tension is

$$T_i = \left(1 - \frac{dt}{B}\left(K_{SE} + K_{PE}\right)\right)T_{i-1} + \frac{dtK_{SE}}{B}\left(K_{PE}\left(L_i - L_{rest}\right) + B\frac{L_i - L_{i-1}}{dt} + A_{m,i}A_{l,i}\right).$$

At each timestep, the previous tension value, T_{i-1}, is multiplied by a constant. To prevent asymptotic instability (i.e. oscillations that cause the tension to increase boundlessly), this constant must be bounded. These linear constraints ensure that the physics timestep constraint,

$$\frac{2B}{K_{SE} + K_{PE}} \geq dt,$$

is true for all muscles. This limitation is described in more detail in a 2020 Living Machines paper.

2. ST Parameter Calculation

The activation parameter, A_m, represents a sigmoidal relationship between stimulus and tension which is important for controlling muscles by applying voltage to the motoneuron. Specifically, the maximum value of A_m (ST_{max}) and the steepness of the ST slope have the largest impact on the relationship between stimulus and tension. The stimulus-tension equation takes the form

$$A_m(V) = \frac{ST_{max}}{1 + e^{S(x_{off} - V)}} + y_{off},$$

where S is steepness, x_{off} is the voltage offset (set to -50mV for all muscles), V is the motoneuron voltage, and y_{off} is the output offset. The range for the ST-curve is defined as [-60, 40] mV in order to interface with functional subnetwork neurons defined from prior work (Szczecinski, Hunt, and Quinn 2017).

Originally, I set the ST output range to [0, $1.05F_{max}$] and then determined the necessary stiffness for each muscle. The motivation for this method was to establish a range in which ST_{max} was slightly larger than F_{max} with the belief that the A_m parameter would then be able to generate all values up to the maximum tension. However, these values required a curve steepness that was quite large (~1200), resulting in a steep curve with a form similar to that in Figure 9.

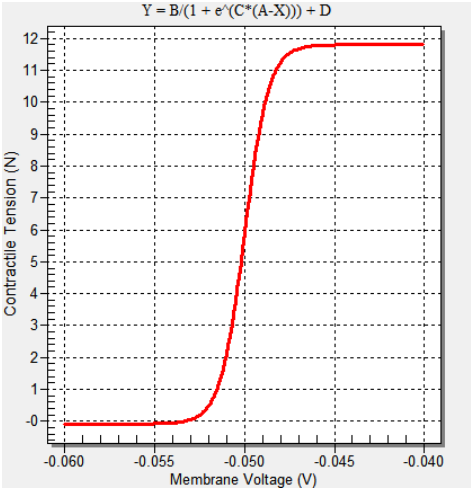

Figure 9 A steeper ST-curve causes the muscle to behave like a switch.

The issues with a steep ST-curve using the output values as defined above are twofold. First, the tension generating capabilities of motoneuron stimulation are inhibited by a term in the tension equation which reduces the output range of the ST-curve. Second, the steeper the ST-curve is, the more it behaves like a switch.

When running experiments where the hindlimb is actuated by muscle stimulation, I noticed that the maximum tension for any muscle was much smaller than F_{max}. This limited the tension output and made the leg weaker than it could be. The reduced output is related to the term $-\left(1+\frac{K_{PE}}{K_{SE}}\right)T$ in the tension equation. Essentially, this term inhibits tension generation, while A_m is trying to increase it. To address this issue, the value of ST_{max} is dynamically set based on the viscoelastic parameters of the muscle in order to balance the inhibitory tension term with the activation term.

Steady state muscle tension is a function of length and activation,

$$T^*(L,A_m)=\left(\frac{K_{SE}}{K_{SE}+K_{PE}}\right)\left(K_{PE}\lceil L-L_{rest},0\rceil+A_l(L)A_m\right). \quad 4$$

At resting length ($L = L_r$), the steady state tension becomes

$$T^*(A_m) = \left(\frac{K_{SE}}{K_{SE} + K_{PE}} \right) A_m . \qquad 5$$

To generate maximal tension through motoneuron activation, the ST_{max} is set such that

$$ST_{max} = \frac{K_{SE} + K_{PE}}{K_{SE}} F_{max} .$$

This assumes that at steady-state resting position, the muscle can generate F_{max} by stimulating the motoneuron. This approach can create values of ST_{max} that are dramatically larger than F_{max}, exacerbating the switch-like behavior related to curve steepness.

It is difficult to create smooth motoneuron-driven motion with a steep curve because muscle tension tends to switch on and off rather than gradually shift values during stride. However, any reduction in curve steepness also means that the output range of the ST curve will be reduced. I decided to reduce the switch-like behavior of the ST curve by reducing the ST-curve output range slightly to [0, $.98ST_{max}$]. To find the necessary steepness for this range, we solve equations at the end values.

$$A_m(-60mV) = 0 \qquad A_m(-40mV) = .98ST_{max}$$

$$\frac{ST_{max}}{1 + e^{.01S}} + y_{off} = 0 \qquad \frac{ST_{max}}{1 + e^{-.01S}} + y_{off} = .98ST_{max}$$

$$\frac{1}{1 + e^{-.01S}} - \frac{1}{1 + e^{.01S}} = .98$$

which results in values of $S = 459.5$ and $y_{off} = -.01ST_{max}$. Now, when I set K_{se}, K_{pe}, and B for each muscle, I also set $ST_{max} = \frac{K_{SE} + K_{PE}}{K_{SE}} F_{max}$, $y_{off} = -.01ST_{max}$, and S = 459.5.

References

Aoi, Shinya, Takahiro Kondo, Naohiro Hayashi, Dai Yanagihara, Sho Aoki, Hiroshi Yamaura, Naomichi Ogihara, et al. 2013. "Contributions of Phase Resetting and Interlimb Coordination to the Adaptive Control of Hindlimb Obstacle Avoidance during Locomotion in Rats: A Simulation Study." *Biological Cybernetics* 107 (2): 201–16. https://doi.org/10.1007/s00422-013-0546-6.

Beer, Randall D., Hillel J. Chiel, and John C. Gallagher. 1999. "Evolution and Analysis of Model CPGs for Walking: II. General Principles and Individual Variability." *Journal of Computational Neuroscience* 7 (2): 119–47. https://doi.org/10.1023/A:1008920021246.

Charles, James P., Ornella Cappellari, Andrew J. Spence, Dominic J. Wells, and John R. Hutchinson. 2016. "Muscle Moment Arms and Sensitivity Analysis of a Mouse Hindlimb Musculoskeletal Model." *Journal of Anatomy* 229 (4): 514–35. https://doi.org/10.1111/joa.12461.

Chiel, Hillel J., and Randall D. Beer. 1997. "The Brain Has a Body: Adaptive Behavior Emerges from Interactions of Nervous System, Body and Environment." *Trends in Neurosciences* 20 (12): 553–57. https://doi.org/10.1016/S0166-2236(97)01149-1.

Chiel, Hillel J., Randall D. Beer, and Leon S. Sterling. 1988. "Heterogeneous Neural Networks for Adaptive Behavior in Dynamic Environments." In *Proceedings of the 1st International Conference on Neural Information Processing Systems*, 577–585. NIPS'88. Cambridge, MA, USA: MIT Press. http://dl.acm.org/citation.cfm?id=2969735.2969802.

Chiel, Hillel J., Lena H. Ting, Örjan Ekeberg, and Mitra J. Z. Hartmann. 2009. "The Brain in Its Body: Motor Control and Sensing in a Biomechanical Context." *Journal of Neuroscience* 29 (41): 12807–14. https://doi.org/10.1523/JNEUROSCI.3338-09.2009.

Cofer, David, Gennady Cymbalyuk, William J. Heitler, and Donald H. Edwards. 2010. "Control of Tumbling during the Locust Jump." *Journal of Experimental Biology* 213 (19): 3378–87. https://doi.org/10.1242/jeb.046367.

Cofer, David, Gennady Cymbalyuk, James Reid, Ying Zhu, William J. Heitler, and Donald H. Edwards. 2010. "AnimatLab: A 3D Graphics Environment for Neuromechanical Simulations." *Journal of Neuroscience Methods* 187 (2): 280–88. https://doi.org/10.1016/j.jneumeth.2010.01.005.

Crowninshield, Roy D., and Richard A. Brand. 1981. "A Physiologically Based Criterion of Muscle Force Prediction in Locomotion." *Journal of Biomechanics* 14 (11): 793–801. https://doi.org/10.1016/0021-9290(81)90035-X.

Eng, Carolyn M., Laura H. Smallwood, Maria Pia Rainiero, Michele Lahey, Samuel R. Ward, and Richard L. Lieber. 2008. "Scaling of Muscle Architecture and Fiber Types in the Rat Hindlimb." *Journal of Experimental Biology* 211 (14): 2336–45. https://doi.org/10.1242/jeb.017640.

Full, R. J., and D. E. Koditschek. 1999. "Templates and Anchors: Neuromechanical Hypotheses of Legged Locomotion on Land." *Journal of Experimental Biology* 202 (23): 3325–32.

Greene, E. C. 1955. *Anatomy of the Rat.* New York: Hafner Publishing Co. https://www.cabdirect.org/cabdirect/abstract/19561405416.

Hill Archibald Vivian. 1938. "The Heat of Shortening and the Dynamic Constants of Muscle." *Proceedings of the Royal Society of London. Series B - Biological Sciences* 126 (843): 136–95. https://doi.org/10.1098/rspb.1938.0050.

Hof, A. L. 2001. “The Force Resulting from the Action of Mono- and Biarticular Muscles in a Limb.” *Journal of Biomechanics* 34 (8): 1085–89. https://doi.org/10.1016/S0021-9290(01)00056-2.

Hooper, Scott L. 2012. “Body Size and the Neural Control of Movement.” *Current Biology* 22 (9): R318–22. https://doi.org/10.1016/j.cub.2012.02.048.

Hooper, Scott L., Christoph Guschlbauer, Marcus Blümel, Philipp Rosenbaum, Matthias Gruhn, Turgay Akay, and Ansgar Büschges. 2009. “Neural Control of Unloaded Leg Posture and of Leg Swing in Stick Insect, Cockroach, and Mouse Differs from That in Larger Animals.” *Journal of Neuroscience* 29 (13): 4109–19. https://doi.org/10.1523/JNEUROSCI.5510-08.2009.

Hunt, Alexander. 2016. “Neurologically Based Control for Quadruped Walking.” Cleveland, OH: Case Western Reserve University.

Hunt, Alexander, Manuela Schmidt, Martin Fischer, and Roger D. Quinn. 2014. “Neuromechanical Simulation of an Inter-Leg Controller for Tetrapod Coordination.” In *Biomimetic and Biohybrid Systems*, edited by Armin Duff, Nathan F. Lepora, Anna Mura, Tony J. Prescott, and Paul F. M. J. Verschure, 142–53. Lecture Notes in Computer Science. Springer International Publishing.

Hunt, Alexander, Nicholas S. Szczecinski, Emanuel Andrada, Martin Fischer, and Roger D. Quinn. 2015. “Using Animal Data and Neural Dynamics to Reverse Engineer a Neuromechanical Rat Model.” In *Biomimetic and Biohybrid Systems*, edited by Stuart P. Wilson, Paul F.M.J. Verschure, Anna Mura, and Tony J. Prescott, 211–22. Lecture Notes in Computer Science. Springer International Publishing.

Johnson, W. L., D. L. Jindrich, H. Zhong, R. R. Roy, and V. R. Edgerton. 2011. “Application of a Rat Hindlimb Model: A Prediction of Force Spaces Reachable Through Stimulation of Nerve Fascicles.” *IEEE Transactions on Biomedical Engineering* 58 (12): 3328–38. https://doi.org/10.1109/TBME.2011.2106784.

Kaufman, K. R., K. -N. An, W. J. Litchy, and E. Y. S. Chao. 1991. “Physiological Prediction of Muscle Forces—I. Theoretical Formulation.” *Neuroscience* 40 (3): 781–92. https://doi.org/10.1016/0306-4522(91)90012-D.

Lee, Sang Wook, Hua Chen, Joseph D. Towles, and Derek G. Kamper. 2008. “Estimation of the Effective Static Moment Arms of the Tendons in the Index Finger Extensor Mechanism.” *Journal of Biomechanics* 41 (7): 1567–73. https://doi.org/10.1016/j.jbiomech.2008.02.008.

Markin, Sergey N., Michel A. Lemay, Boris I. Prilutsky, and Ilya A. Rybak. 2012. “Motoneuronal and Muscle Synergies Involved in Cat Hindlimb Control during Fictive and Real Locomotion: A Comparison Study.” *Journal of Neurophysiology* 107 (8): 2057–71. https://doi.org/10.1152/jn.00865.2011.

McCrea, David A., and Ilya A. Rybak. 2008. “Organization of Mammalian Locomotor Rhythm and Pattern Generation.” *Brain Research Reviews*, Networks in Motion, 57 (1): 134–46. https://doi.org/10.1016/j.brainresrev.2007.08.006.

Nishikawa, Kiisa, Andrew A. Biewener, Peter Aerts, Anna N. Ahn, Hillel J. Chiel, Monica A. Daley, Thomas L. Daniel, et al. 2007. “Neuromechanics: An Integrative Approach for Understanding Motor Control.” *Integrative and Comparative Biology* 47 (1): 16–54. https://doi.org/10.1093/icb/icm024.

O’Neill, Matthew C., Leng-Feng Lee, Susan G. Larson, Brigitte Demes, Jack T. Stern, and Brian R. Umberger. 2013. “A Three-Dimensional Musculoskeletal Model of the Chimpanzee

(Pan Troglodytes) Pelvis and Hind Limb." *Journal of Experimental Biology* 216 (19): 3709–23. https://doi.org/10.1242/jeb.079665.

Pedotti, A., V. V. Krishnan, and L. Stark. 1978. "Optimization of Muscle-Force Sequencing in Human Locomotion." *Mathematical Biosciences* 38 (1): 57–76. https://doi.org/10.1016/0025-5564(78)90018-4.

Penrod, D.D., D.T. Davy, and D.P. Singh. 1974. "An Optimization Approach to Tendon Force Analysis." *Journal of Biomechanics* 7 (2): 123–29. https://doi.org/10.1016/0021-9290(74)90050-5.

Pfeifer, Rolf, Max Lungarella, and Fumiya Iida. 2007. "Self-Organization, Embodiment, and Biologically Inspired Robotics." *Science* 318 (5853): 1088–93. https://doi.org/10.1126/science.1145803.

Prilutsky, Boris I., Alexander N. Klishko, Douglas J. Weber, and Michel A. Lemay. 2015. "Computing Motion Dependent Afferent Activity During Cat Locomotion Using a Forward Dynamics Musculoskeletal Model." In *Neuromechanical Modeling of Posture and Locomotion*. Springer.

Prilutsky, Boris I., and Vladimir M. Zatsiorsky. 2002. "Optimization-Based Models of Muscle Coordination." *Exercise and Sport Sciences Reviews* 30 (1): 32.

Sandercock, Thomas G., Qi Wei, Yasin Y. Dhaher, Dinesh K. Pai, and Matthew C. Tresch. 2018. "Vastus Lateralis and Vastus Medialis Produce Distinct Mediolateral Forces on the Patella but Similar Forces on the Tibia in the Rat." *Journal of Biomechanics* 81 (November): 45–51. https://doi.org/10.1016/j.jbiomech.2018.09.007.

Shadmehr, Reza, and Michael A. Arbib. 1992. "A Mathematical Analysis of the Force-Stiffness Characteristics of Muscles in Control of a Single Joint System." *Biological Cybernetics* 66 (6): 463–77. https://doi.org/10.1007/BF00204111.

Szczecinski, Nicholas S., Andrew P. Getsy, Joshua P. Martin, Roy E. Ritzmann, and Roger D. Quinn. 2017. "Mantisbot Is a Robotic Model of Visually Guided Motion in the Praying Mantis." *Arthropod Structure & Development*, From Insects to Robots, 46 (5): 736–51. https://doi.org/10.1016/j.asd.2017.03.001.

Szczecinski, Nicholas S., Alexander J. Hunt, and Roger D. Quinn. 2017. "A Functional Subnetwork Approach to Designing Synthetic Nervous Systems That Control Legged Robot Locomotion." *Frontiers in Neurorobotics* 11. https://doi.org/10.3389/fnbot.2017.00037.

Thota, Anil K., Sonia Carlson Watson, Elizabeth Knapp, Brian Thompson, and Ranu Jung. 2005. "Neuromechanical Control of Locomotion in the Rat." *Journal of Neurotrauma* 22 (4): 442–65. https://doi.org/10.1089/neu.2005.22.442.

Torres-Oviedo, Gelsy, Jane M. Macpherson, and Lena H. Ting. 2006. "Muscle Synergy Organization Is Robust Across a Variety of Postural Perturbations." *Journal of Neurophysiology* 96 (3): 1530–46. https://doi.org/10.1152/jn.00810.2005.

Twickel, Arndt von, Christoph Guschlbauer, Scott L. Hooper, and Ansgar Büschges. 2019. "Swing Velocity Profiles of Small Limbs Can Arise from Transient Passive Torques of the Antagonist Muscle Alone." *Current Biology* 29 (1): 1-12.e7. https://doi.org/10.1016/j.cub.2018.11.016.

Visser, J. J., J. E. Hoogkamer, M. F. Bobbert, and P. A. Huijing. 1990. "Length and Moment Arm of Human Leg Muscles as a Function of Knee and Hip-Joint Angles." *European Journal of Applied Physiology and Occupational Physiology* 61 (5): 453–60. https://doi.org/10.1007/BF00236067.

Vogel, Steven. 2005. “Living in a Physical World III. Getting up to Speed.” *Journal of Biosciences* 30 (3): 303–12. https://doi.org/10.1007/BF02703667.

Williams, S. B., A. M. Wilson, L. Rhodes, J. Andrews, and R. C. Payne. 2008. “Functional Anatomy and Muscle Moment Arms of the Pelvic Limb of an Elite Sprinting Athlete: The Racing Greyhound (Canis Familiaris).” *Journal of Anatomy* 213 (4): 361–72. https://doi.org/10.1111/j.1469-7580.2008.00961.x.

Yeo, Sang Hoon, Christopher H. Mullens, Thomas G. Sandercock, Dinesh K. Pai, and Matthew C. Tresch. 2011. “Estimation of Musculoskeletal Models from in Situ Measurements of Muscle Action in the Rat Hindlimb.” *Journal of Experimental Biology* 214 (5): 735–46. https://doi.org/10.1242/jeb.049163.

Zajac, F. E. 1989. “Muscle and Tendon: Properties, Models, Scaling, and Application to Biomechanics and Motor Control.” *Critical Reviews in Biomedical Engineering* 17 (4): 359–411.